Limitations of optical reticle inspection for 45nm node and beyond

S. Teuber, A. Bzdurek, A.C. Dürr, J. Heumann, C. Holfeld

Advanced Mask Technology Center GmbH & Co. KG, Raehnitzer Allee 9, D-01109 Dresden, Germany

ABSTRACT

Pushing the limits of optical lithography by immersion technology requires ever smaller feature sizes on the reticle. At the same time the k1-factor will be shifted close to the theoretical limit, e.g. the OPC structures on the reticle become very aggressive. For the mask shop it is essential to manufacture defect free masks. The minimum defect size, which needs to be found reliably, becomes smaller with decreasing feature sizes. Consequently optical inspection of masks for the 45nm node and below will be challenging.
In this paper the limits of existing KLA inspection tools were investigated by systematic inspection of different structures without and with programmed defects. A test mask with isolated and dense lines/space patterns including programmed defects was manufactured, completely characterized by CD-SEM and inspected with state-of-the-art inspection system. AIMS^{TM} measurements were used to evaluate the defect printing behavior. The analysis of the measurement data gives an input for requirements of reticle inspection of upcoming 45nm node and beyond.

Keywords: 45nm, inspection, AIMS, optical masks, binary masks, KLA

1. INTRODUCTION

With continued shrinkage of feature sizes the application of 193nm exposure systems with high numerical aperture (NA), and the use of resolution enhancement technologies (RET) have become essential for obtaining the desired pattern accuracy on wafer. The introduction of immersion technology opens the opportunity for further extension of ArF optical lithography. The complexity and volume of data required for mask writing have been rapidly increased because the pattern exposure systems have been performing under the constraint of low k1-factor. The required masks are becoming more and more complex at smaller feature sizes due to RET, like sub-resolution assist features or complex OPC features. This required mask pattern complexity is making mask inspection increasingly more difficult [1]. In order to catch target defects it is highly desirable to increase the sensitivity of the inspection system. The high inspection tool sensitivity in combination with the small features may result in tool related defects (false defects), which are not real. As this occurs in a regime, which is often not characterized and therefore not specified by the tool vendor, a new test mask was designed.

In a real production environment it is mandatory of having the mask inspected with three different methods:

1. Die-to-die (under the constraint of having identical chips)
2. Die-to-database (pattern defect inspection);
3. Starlight (particle inspection).

When using one of those inspection methods, there are two sets of factors, which influence the capability of defect detection:

A) Factors, related to an instrumental limit caused by the mask inspection system:
   a. Pixel size;
   b. Algorithm;
   c. Sensitivity levels;
B) Factors, related to the reticle patterning process:

Photomask Technology 2006, edited by Patrick M. Martin, Robert J. Naber,
Proc. of SPIE Vol. 6349, 63490T, (2006) · 0277-786X/06/$15 · doi: 10.1117/12.686078

a. Mask features size and duty cycle which limit the optical contrast in the optical microscope;
b. Mask induced polarization effects [2];
c. Line edge roughness of mask features;
d. Non-linear feature size scaling due to non-linear patterning process;
e. Feature size errors due to the inaccuracy of reticle patterning process;

In order to differentiate between those factors influencing the defect inspection capability an inspection analysis with a test mask having a special layout was performed. The obtained results will be discussed in the following sections.

2. TEST MASK PRODUCTION AND CHARACTERIZATION

A completely new design was developed at the Advanced Mask Technology Center (AMTC). A systematic variation of dense lines and space arrays as well as dense contact hole/dot arrays is distributed over the mask. Furthermore some special patterns required for additional studies were included in the design. This design need to fulfill some important boundary conditions:

1. The design needs to be compatible to the standard mask house pattern set (alignment or calibration marks);
2. The pattern loading needs to be as homogeneous as possible;
3. The mask needs to be inspectable in all 3 inspection modes;
4. The complexity of the design needs to be increasing when going from bottom to top of the mask;
5. Small features for CD uniformity analysis need to be included.
6. Features for registration analysis need to be included.
7. Programmed defects with varying defect size, defect type and feature size of the base structures need to be included.

After successful creation of the design a full set of measurement recipes were developed:

- Critical dimension (CD) measurements;
- Placement accuracy measurements (REG);
- Line width roughness measurements (LWR);
- Mask inspection in all 3 modes: die-to-die, die-to-database, starlight (D2D, D2DB, SL)
- AIMS defect disposition measurements (AIMS).

A set of test masks was produced using the standard production processes of record having different materials and resist types. In the following the results of standard chrome on glass (CoG) mask using a standard NTAR7 blank from Hoya with positive resist FEP171 are presented.

An important information for the inspection measurement system when measuring in the die-to-database mode is the linearity behavior of the mask pattern feature sizes, because the captured image of the mask will be compared to the design data. However, the production process changes the features sizes. That's why the linearity information would help to calibrate the design data. In Figure 1 the difference between measured and design CD of clear features are shown as function of measured CD. There are two regions observable. In the first region of small feature size a dramatic change of the CD off-target occurs, whereas in the region of larger feature sizes the off-target stays approximately constant. An important fact is that the scattering of the linearity curve is rather small. This small variation increases the confidence in predicting the final mask features size from the design feature sizes.

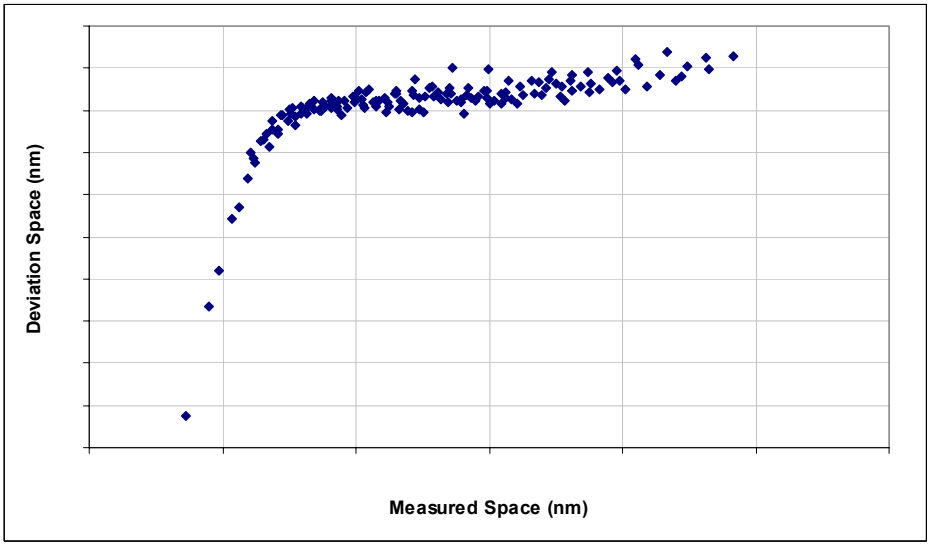

Figure 1: Linearity behavior of dense lines and space arrays on the inspection test mask.

After analyzing of all lines/space CD measurements we were able to extract the smallest structures which are resolved. The data set was very carefully analyzed in order to sort out all measurement errors. From that analysis we are confident, that the resolution limit is smaller than 40nm for dark lines and smaller 100nm for clear spaces. The corresponding SEM pictures of the smallest structures are shown in Figure 2.

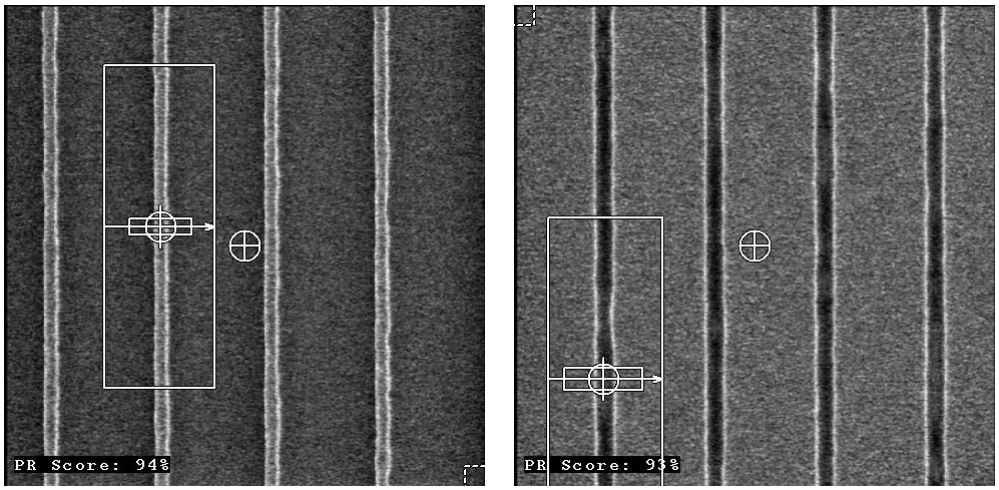

Figure 2: SEM overview pictures taken with AMAT SEM tool showing the observed smallest line (left picture) and the smallest space (right picture).

Furthermore, we analyzed the CD uniformity distribution over the plate in order to control the mask pattern quality. We measured the CDU of isolated clear structures with sizes ranging from 400 down to 160nm. The resulting CDU values are shown in Table 1 and ranging from 2.9nm to 3.6nm. Figure 3 shows the corresponding bubble plot.

	Clear 1	**Clear 2**	**Clear 3**	**Clear 4**	**Clear 5**	**Clear 6**
CD	160nm	190nm	230nm	270nm	340nm	390nm
3 sigma	3.5nm	3.5nm	3.0nm	3.6nm	3.0nm	2.9nm

Table 1: CD uniformity values of isolated clear line structures measured on CoG test mask.

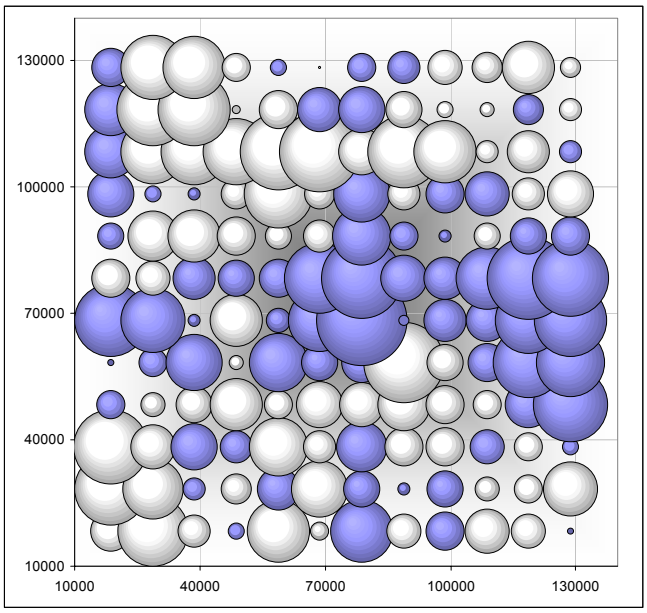

Figure 3: CD uniformity bubble plot of 340nm isolated clear line structures distributed over the mask. The 3-sigma deviation is smaller than 3nm.

3. INSPECTION RESULTS AND DISCUSSION

The test mask described above was inspected on a KLA 576 using the P90 pixel. Three different inspection modes were tested: die-to-die (D2D), die-to-database (D2Db), and Starlight (SL). To determine the limits of the P90 pixel in combination with the respective algorithm, the sensitivity settings were kept at maximum (100) for each respective detector.
For the KLA 576 the inspection scanning progresses from bottom to top. For the ease of inspection the mask was rotated such that the largest features were inspected first. As the features became smaller the tool started triggering defects. Once a total defect count of 3000 was exceeded, the inspection was stopped and saved, in order to limit the inspection report file size.
The inspection reports were reviewed and the defects classified into two categories:

1. Mask related (real) defect;
2. Tool generated (false) defect, which is not present on the mask;

Depending on the defect density the individual areas (constant line/pitch ratio and constant pitch) were separated into three categories

1. Inspectable (defect density < 1 defect/mm^2)
2. Non-inspectable due to real defects
3. Non-inspectable due to false defects
4. Structures not resolved based on SEM images

The results for all three inspection modes were drawn into a diagram. From top to bottom the ratio between the line-width and pitch (duty cycle) is drawn ranging from 0.9 to 0.1. From left to right the wafer half pitch decreases from 65nm to 40nm.

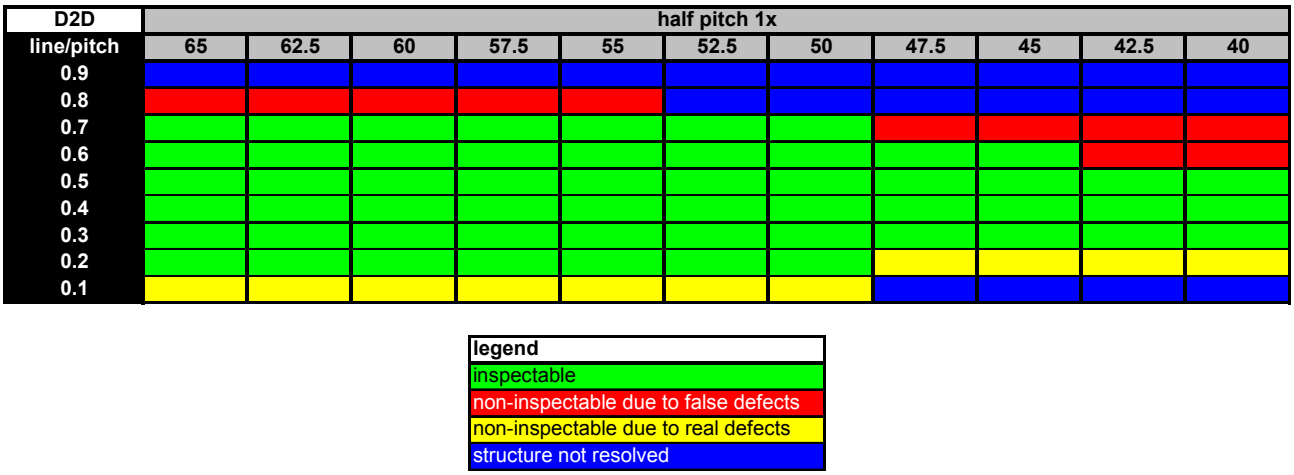

Figure 4: Schematic overview of the D2D inspection results divided into 4 categories (see legend on the right-hand side).

The results of the D2D inspection are displayed in Figure 4. For very small clear lines (lines/pitch 0.9 to approx. 0.6) the tool triggers excessively false defects. These false defects are caused by an alignment error between the test and reference image.
The KLA 5xx inspection algorithm compares the test (see Figure 5, left) and reference image (middle). Due to limited stage accuracy the test and reference images first need to be aligned by a here-in called aligner. Thereafter a so-called difference images is generated (right). Finally, a defect detection algorithm locates deviations from nominal (right).

Figure 5: Test (left), reference (middle), and difference image (right) of a false defect triggered by the D2D algorithm

The aligner extracts certain image information in order to align the images properly. It requires a certain contrast of the test and reference images. In turn once the image contrast falls below a certain value the images are not necessarily aligned correctly (see Figure 5, compare left and middle). The resulting difference image (right) shows subsequently a pronounced difference at the last line position, which thereafter are triggered by the defect detection algorithm.
For the D2D algorithm this lower image contrast threshold is exceeded at a line/pitch ratio of approximately 0.6. For all line/pitch ratios above the tool triggers massively false defects.
For comparison, in Figure 6 the inspection contrast is shown as a function of the mask half pitch (4x). It emphasizes that the above described image contrast loss is a function of the half pitch as well as of the duty cycle of the mask structures. Since the inspection system is an optical system this contrast behavior can be described by a limited numerical aperture. If the optical parameters are known this contrast behavior could be predicted by optical simulations.

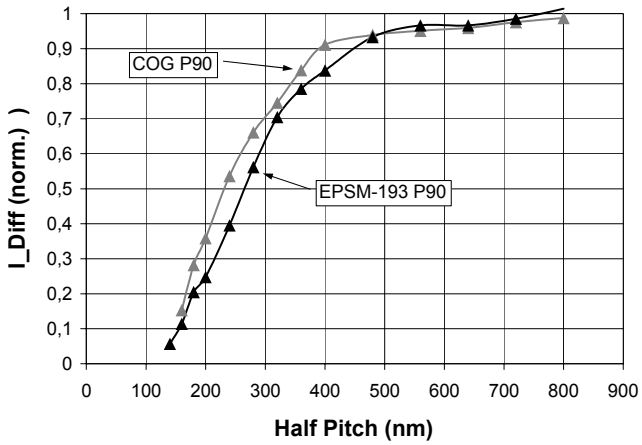

Figure 6: Inspection contrast as function of half pitch of dense lines structures (1:1) as measured on the KLA 576 pattern inspection system with pixel P90. The contrast is gradually reduced below a half pitch of 500nm. The pattern can be inspected only above a minimum contrast.

For line/pitch ratio below 0.6 all pitches ranging from 65nm to 40nm are inspectable meaning the defect density is below 1 defect/cm^2. Only for line/pitch ratios below 0.2 a large number of real defects are triggered due to the lines having large line edge roughness or being either not properly resolved or not present.

D2DB	half pitch 1x										
line/pitch	65	62.5	60	57.5	55	52.5	50	47.5	45	42.5	40
0.9											
0.8											
0.7											
0.6											
0.5											
0.4											
0.3											
0.2											
0.1											

Figure 7: Schematic overview of the D2Db inspection results divided into four categories. The color code is defined in the legend of Figure 4.

Figure 7 shows the D2Db inspection results. The diagram is very similar to the D2D inspection diagram. As for the D2D algorithm the aligner fails above a line/pitch ratio 0.6. The only difference is observed for line/pitch ratios of 0.2, which are still D2Db inspectable. This is caused by a slightly lower defect sensitivity of the D2Db algorithm compared to the D2D algorithm.

SL	half pitch 1x										
line/pitch	65	62.5	60	57.5	55	52.5	50	47.5	45	42.5	40
0.9											
0.8											
0.7											
0.6											
0.5											
0.4											
0.3											
0.2											
0.1											

Figure 8: Schematic overview of the SL inspection results divided into four categories. The color code is defined in the legend of Figure 4.

Figure 8 shows the SL inspection results. The inspection was only possible for line/pitch ratios between 0.5 and 0.3. Above 0.5 and below 0.3 false defects were triggered due to limitations of the SL2-algorithm.
For the KLA 5xx platform, a new SL2 algorithm was introduced. Based on the transmitted and reflected image (see Figure 9 left images) and the known optical behavior of the blank materials (quartz, chrome, MoSi) the algorithm models a reference transmitted and reflected light image (middle images). Out of the test and reference images a difference image for transmitted and reflected light is generated (right images). The defect detection algorithm again searches for any deviation from the nominal.

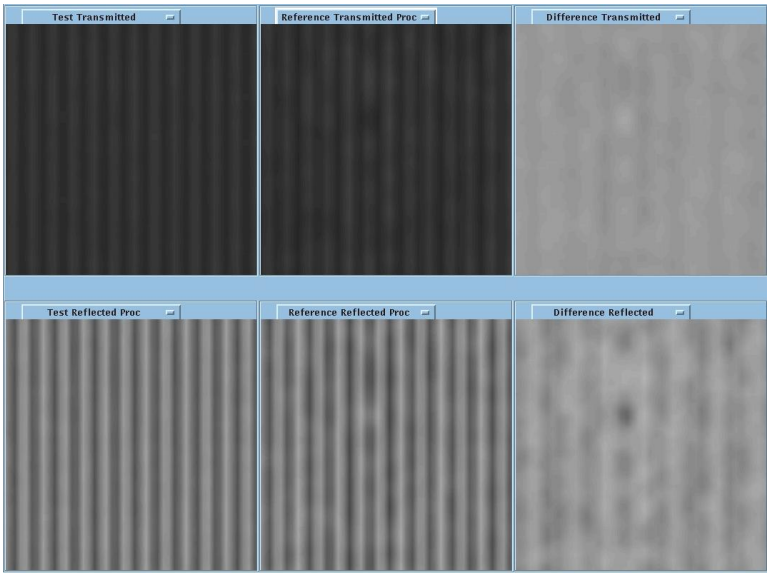

Figure 9: Test transmitted (left top), reference transmitted (middle top), and difference transmitted (right top) as well as respective reflected images (bottom images) of a false defect triggered by the SL2 algorithm

Due to poor image contrast of the test transmitted image (top left) the modeling of the reference images generates faulty reference images (middle images). The subsequent difference images (right images) show image variations, which are not real and causes the defect detection algorithm to trigger false defects.
For line/pitch ratios above 0.5 the low transmitted image contrast causes the SL2-algorithm to malfunction. In turn for line/pitch ratios below 0.3 the low reflected image contrast causes the SL2-alogrithm to malfunction.

The image contrast plays a key role for all inspection modes, which limits the inspectability of certain mask features due to different mechanisms. The image contrast for equally spaced lines & spaces (line/pitch ratio equal to 0.5) has been measured in a previous study [1]. Based on the current results the KLA 5xx can inspect pattern down to an image contrast of approx. 0.4. Below this value false defects a likely to be triggered.

4. INSPECTION AND AIMS CHARACTERIZATION OF PROGRAMMED DEFECTS

After investigation of inspection limits on dense line/space arrays the defect inspection sensitivity as a function of half pitch is of general interest [3]. Since the contrast of the optical microscope in the inspection tool decreases with decreasing half pitch a different defect capture rate is expected. On the test mask a set of vertical dense lines and space arrays with line/pitch ratio of 0.5 and varying pitch including programmed defects was placed. 10 different defect types in both tones with varying defect size were uniformly distributed in each individual l/s array. The defect size was changed from 1%-100% normalized to the actual half pitch for comparison reasons. 10 inspection runs were performed on each individual l/s array in die-to-die mode. A chip with programmed defects was compared with a chip without programmed defects. The smallest defect size where the inspection capture rate reaches full capability value (100%) is of interest and is illustrated in Figure 10. There is a strong dependence of the capture rate on the defect type observable. The observed capture rate is strongly dominated by the aspect ratio for extension-x/1 defects ($x \geq 1$, e.g. $size_x > size_y$).

Since the extension-1/y defects (y≥1) were too big, no dependence on defect size was observable, i.e. all defects were captured in the inspection. Furthermore, the capture rates of clear and dark defects are quite comparable. The observed capture rate results for oversize und undersize defects are obviously affected by algorithm errors of this method, because no defect was triggered although the CD deviation was 100%. Last, the capture rate of center defects is less compared to the capture rate of extension defects, because the smallest defect size for 100% capture of center defects is nearly double of that of extension defects.

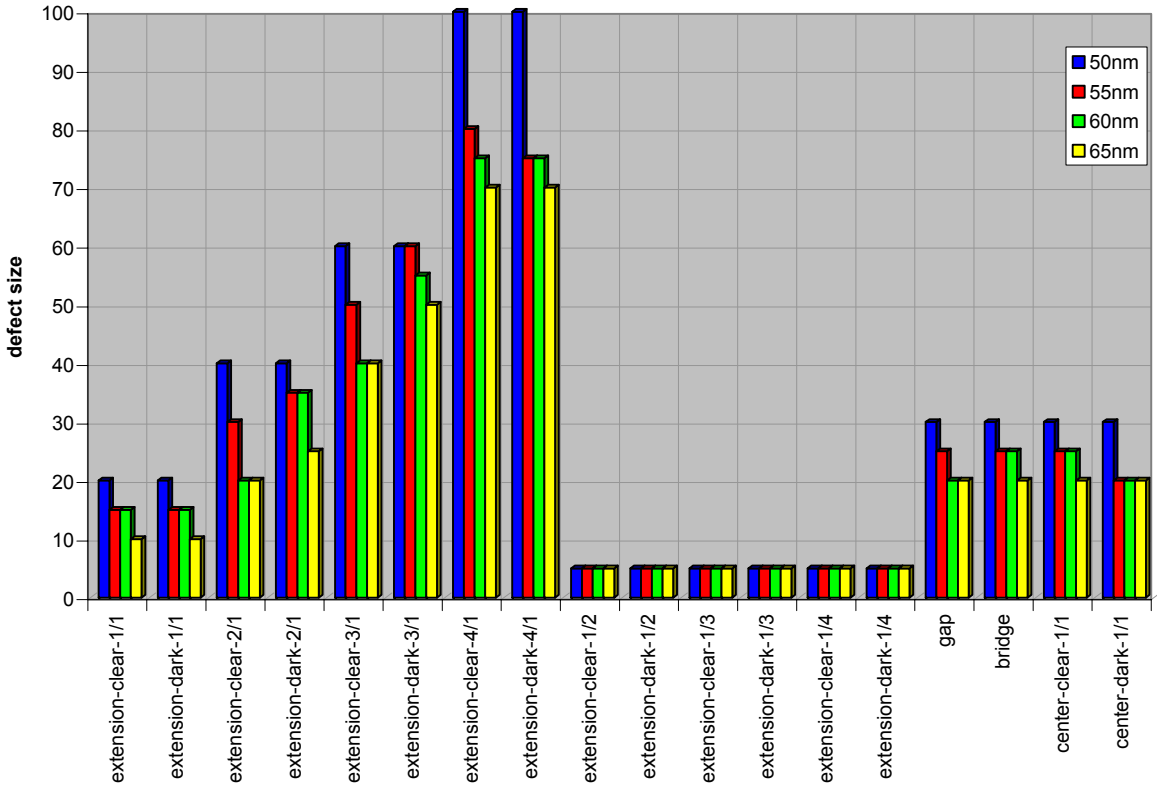

Figure 10: Smallest defect size normalized to half pitch with 100% capture rate as function of half pitch (1x values) of the lines/space arrays for different defect types.

Comparing the capture rate of programmed defects included in l/s arrays with different half pitch, a clear dependence can be observed. For instance, the capture rate decreases or the smallest defect size for 100% capture rate increases for decreasing half pitches. This effect is observable for all defect types except those, where the inspection tool is operated at the detection limit.

Now, the printability behavior of the programmed defects was assessed by measuring the aerial images with a newly developed AIMS45-193i tool from Zeiss, which can measure at NA>1 (maximum NA = 1.4). For the 50nm dense l/s structures NA=1.2 and a dipole illumination was chosen. Since mask polarization effects and vector effects play a role for immersion illumination effect, the AIMS tool provides two different modes: the “standard” mode and the “scanner” mode, where vector and polarization effects are taken into account. The advantage of the scanner mode is at the expense of larger cycle time. In this study we restricted our AIMS measurements on the “standard” mode. Figure 11 shows the measured intensity deviations for various defect types and varying defect size. The “center defect size” was chosen from the observed minimum detected defects size at 100% inspection capture rate (see measurement results in Figure 10). In order to get more statistics the defect size was further varied by ±10% and ±20%. For some defect types those variations were not possible and are left out in the figure. The measurements show, that the measured AIMS intensity deviation increases with increasing defect size. Depending on defect type, a linear or a quadratic behavior was observed.

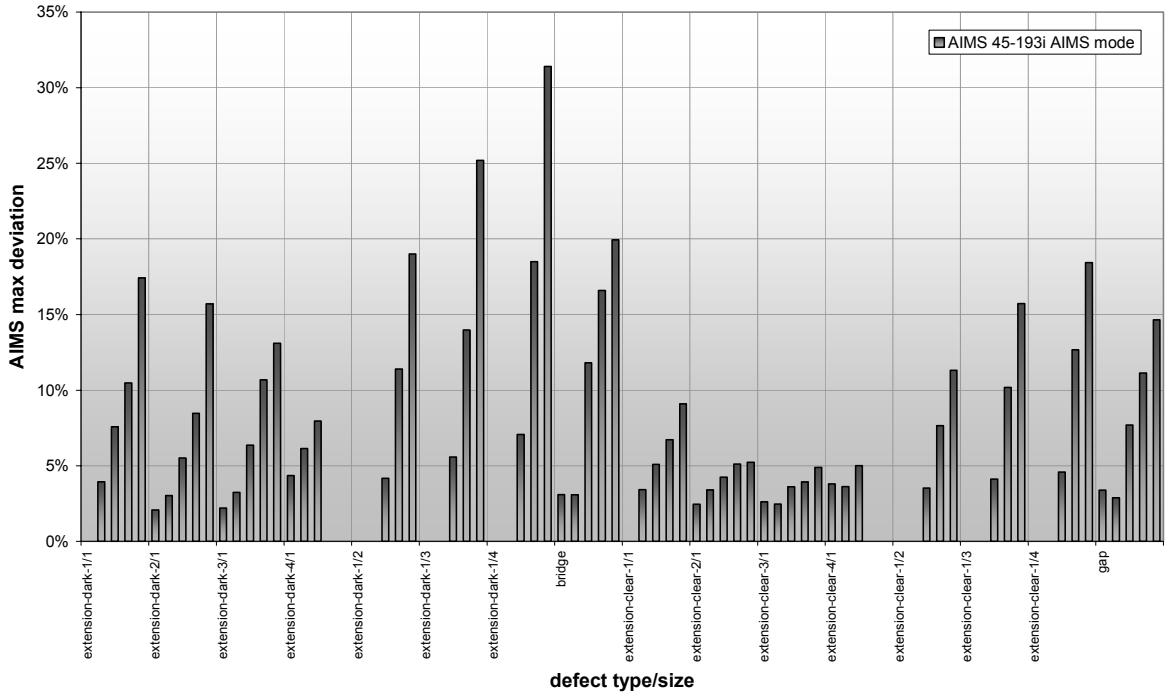

Figure 11: Intensity deviations of programmed defects on 50nm l/s arrays measured with newly developed AIMS45-193i tool under NA=1.2 and dipole illumination settings. The defect size was varied around the minimum defect size at 100% inspection capture rate (taken from Figure 10).

Comparing different defect types, a different printing behavior was observed. While the defect tone plays a minor role, the geometry of the defect types influences significantly the printability. Other influence factors, which could not be measured within this study, like illumination settings, real wafer printing behavior depending on tool and resist, might play also an important role. The measured AIMS intensity deviation is generally a relative number, only. A real printing study, e.g. analyzing the wafer printability of programmed defects for the upcoming 50nm node, will define the maximum allowed AIMS intensity deviation.

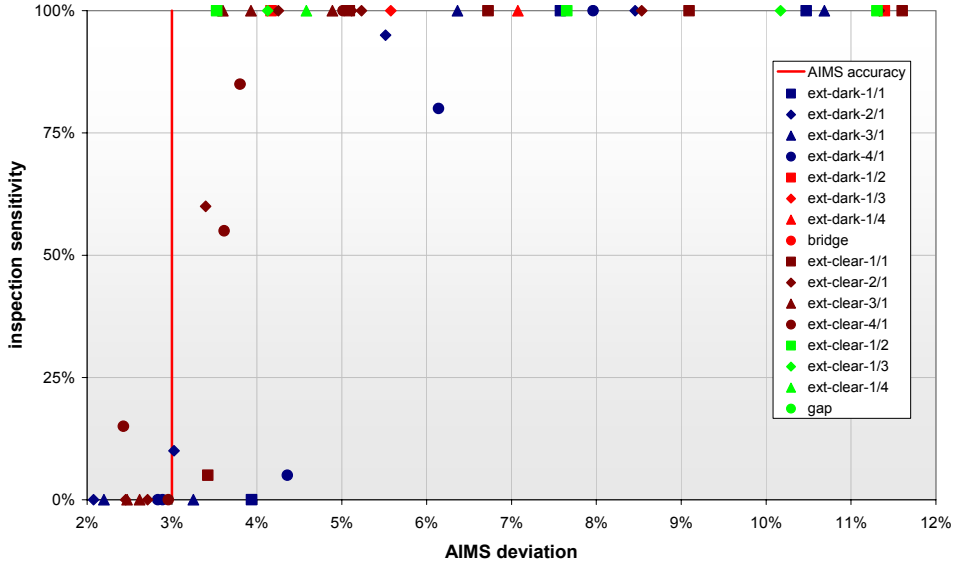

Figure 12: Inspection capture rate as function of measured AIMS intensity deviation for various programmed defect types on 50nm dense l/s arrays. It was assumed, that the AIMS45-193i has a measurement intensity accuracy error of maximum 3%.

In order to investigate the inspection capability, a comparison of the inspection capture rate of the programmed defects with the measured AIMS intensity deviation was performed. Such a plot shows for all defect types for a given maximum AIMS intensity deviation the resulting capture rate. In other words, does the inspection tool capture all defects which will have a significant impact on the printing behavior? The result is illustrated in Figure 12. Assuming a maximum allowed AIMS intensity deviation of 6%, all capture rates except for one defect type (extension-dark-4/1 defect) are 100%. If the AIMS criteria need to be further tightened the capture rate of increasing number of defect types will not approach the 100% line. In this case the inspection capability for 50nm node dense lines/space mask structures is not sufficient and needs further improvement.

In future, a full assessment of the inspection capability needs the inclusion of realistic OPC structures like hammerheads or sub-resolution assist features are required, since their inspection is much more critical and the resulting printing behavior is different, as well. Therefore additional inspections on such structures with systematic variation of type and size need to be performed.

5. SUMMARY AND OUTLOOK

The inspection limitation for all inspection modes were investigated on a set of varying dense lines/space gratings produced on a binary test mask. Two main problems were identified: first, for small clear scatterbar like structures the small contrast in the optical system causing alignment problems and a lot of false defect counts. Second, small dark scatterbar like structures were not perfectly produced on the mask having large line edge roughness or being not fully resolved and causing therefore real defect detections. Only structures having duty cycles measured in the range of 0.3-0.5 line/pitch all inspection modes show no problems down to 40nm node related structures. The capture rate of programmed defects strongly depends on the structure size, e.g. the capture rate decreases for decreasing pitch. For 50nm node structures, the AIMS intensity deviation with dipole illumination of 100% captured defect sizes varies between 4%-8%. Further studies are required, which compare the wafer print results with the inspection capture rates and the measured AIMS deviations are required for determination of printing behavior of programmed defects.

ACKNOWLEDGEMENTS

AMTC is a joint venture of AMD, Infineon and Toppan Photomasks and gratefully acknowledges the financial support of the German Federal Ministry of Education and Research (BMBF) under Contract No. 01M3154A ("Abbildungsmethodiken für nanoelektrische Bauelemente").
Further we would like to thank Axel Zibold and Klaus Böhm from Carl Zeiss Jena for their support during the measurements at the newly developed AIMS45-193i tool.

REFERENCES

1. J. Heumann, et al, Detailed Characterization of Inspection Tools: Capability and Limitations of the KLA 576, BACUS Symposium on Photomask Technology, 2005
2. Silvio Teuber, et al., Determination of mask induced polarization effects occurring in hyper NA immersion lithography; Proc. SPIE Vol. 5754, p. 543-554, Optical Microlithography XVIII, 2005
3. A. Erdmann, et al., Mask defect printing mechanisms for future lithography generations, Proc. SPIE Vol. 6154, 61541C, Optical Microlithography XIX; 2006